Optics Communications 454 (2020) 124515

Contents lists available at ScienceDirect

Optics Communications

journal homepage: www.elsevier.com/locate/optcom

Effects of the ambient medium and structure parameter on the optical properties of tapered silicon nanowire

Jie Tong [a], Minghao Zhang [a], Shuhua Zhang [a], Yuqing Lei [a], Meicheng Li [b], Mingde Qin [c], Yingfeng Li [b,*]

[a] China Electric Power Research Institute, Beijing, 100192, China
[b] State Key Laboratory of Alternate Electrical Power System with Renewable Energy Sources, North China Electric Power University, Beijing, 102206, China
[c] Program of Materials Science and Engineering, University of California, San Diego, CA 92093, USA

ARTICLE INFO

Keywords:
Tapered silicon nanowire
Ambient medium
Structure parameter
Optical property

ABSTRACT

Tapered silicon nanowire (*T-SiNW*) is expected to have a wider application than a cylindrical one in optical sensors, photovoltaics, etc. due to its broadband light-trapping. However, there is little research on the effect of ambient medium and structure parameters on the optical properties of *T-SiNW*. First, based on numerical simulations it is found that, compared with that in air, when a *T-SiNW* is embedded in ambient medium with refraction index of 1.284: the absorbed light by it under given irradiation becomes much less; the scattered light by it shows a wider angular distribution; the nearfield light around it becomes stronger in a wider area. These mean that *T-SiNW* is more desirable for light-trapping in the ambient medium. Then, as the bottom diameter of *T-SiNW* increases, its light-collecting waveband red-shifts; at the same time, its scattered light shows a broadened angular distribution range. Hence, *T-SiNW* with larger bottom diameter is more desirable for light-trapping, especially for longwave light which is sometimes difficult to be utilized in photovoltaic devices. Besides, we found that the light-collecting and -absorption multiples of *T-SiNW* are both proportional to its length approximatively, which provides a very convenient way to regulate its light-trapping performance. The insights in this work are helpful to the design of devices using *T-SiNW* as the main block.

1. Introduction

In the past twenty years, nano-scaled silicon structures have been demonstrated to own special optical properties based on the leaky mode effect [1–3] or the Fano resonance [4,5]. Among them, cylindrical silicon nanowire (*C-SiNW*) shows both excellent light-trapping [6,7] and controllable light intensity distribution [8]. Tapered silicon nanowire (*T-SiNW*) puts up even better light-trapping due to its continuous diameter thus wider resonance wavelengths [9–11]. Silicon nanotube exhibits exceptional light-absorption ability as it possesses both inner and outer light absorbing areas [12]. Therefore, silicon nanostructures demonstrate great prospects in fields like radial-junction silicon/poly(3,4-ethylene dioxythiophene):poly-styrenesulfonate (Si/PEDOT:PSS) solar cells [13,14], photoelectrochemical [15], self-powered nanowire devices [16–18], nanowire photonic circuit elements [19,20], nano-scaled photonics and electronics [21,22], optical waveguide gas sensors [23] and biosensors [24,25].

SiNW is currently the most studied nano-scaled silicon structures. They are able to be fabricated with controllable diameter and length, by vapor–liquid–solid growth method [26,27], or metal-assisted chemical etching method [28–30]; they are also implemented in certain devices [31–34], bringing about improved photoelectronic conversion efficiency [13,35,36], long distance optical transmission [19,20], and high sensing accuracy [23–25]. Meanwhile, the optical properties of *SiNW* have been widely investigated by experimental measures or numerical simulations [7,37–39] for its practical applications; yet there are still many questions awaited to be answered. For example, the excellent light-harvesting ability of *SiNW* has been firmly demonstrated; nevertheless, there is a little investigation on how much of the harvested light could be actually utilized [40]. Some external factors like dielectric environment may impact the optical response of a nanostructure dramatically, but unfortunately, there is a little study on these factors [41]. Nor is there much research on the detailed distribution characteristics and corresponding utilization schemes of the light field in *SiNW* [42]. As a result, further study on the optical properties of *SiNW* is imperative.

As *T-SiNW* is expected to be better than *C-SiNW* in radial Si/PEDOT:PSS heterojunction hybrid solar cells due to its broadband light-trapping [9–11], the effect of PEDOT:PSS has been investigated at first in this work. Then, since there is no specific investigation on the influence of structure parameters on the optical properties of

* Corresponding author.
E-mail address: liyingfeng@ncepu.edu.cn (Y. Li).

https://doi.org/10.1016/j.optcom.2019.124515
Received 9 June 2019; Accepted 3 September 2019
Available online 5 September 2019

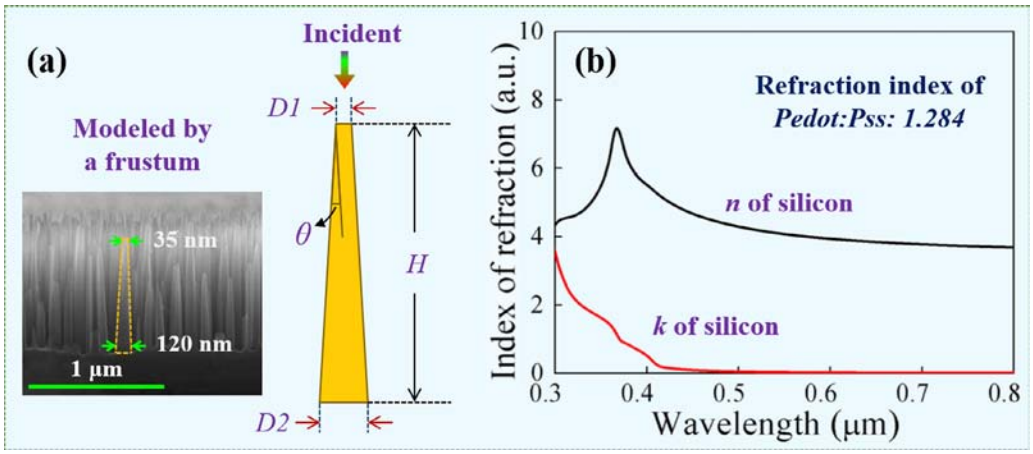

Fig. 1. Model and refraction index of *T-SiNW*. (a) the frustum model; (b) the refraction index of silicon. (For interpretation of the references to colour in this figure legend, the reader is referred to the web version of this article.)

a T-SiNW, the impacts of bottom diameter and height on its light collecting, light absorption, and light scattering features were carefully analyzed. All the studies are carried out using the discrete dipole approximation (DDA) method [43,44], whose reliability has already been well validated [40,42,45]. It is found that *T-SiNW* has less light absorption in PEDOT:PSS than in air; and the cone structure makes the angular distribution of the scattered light wider, being able to convert light from longitudinal transmission to lateral transmission. These two optical features determine that *T-SiNW* is an excellent light-trapping structure, but undesirable for the fabrication of radial-junction photovoltaic devices. In addition, *T-SiNW* with a bottom diameter of 140 nm has the best light-collecting capability; and the light-collecting multiples of it is directly proportional to its length.

2. Model and simulation method

T-SiNW is modeled as a frustum illustrated in Fig. 1(a), according to its real shape as demonstrated by the SEM image in the inset [46]. From the point of preparation, *T-SiNW* has two major variables: the bottom diameter, *D2*, and length, *H*. Therefore, the impacts of *D2* and *H* on the light-management behaviors of *T-SiNW* are mostly investigated. The upper diameter (*D1*) is fixed to be 0.02 μm, but *D2* and *H* vary respectively in an appropriate range, as listed in Table 1. The corresponding cone angle, θ, of each *T-SiNW* is also given. Only top irradiation is taken into account because the light-trapping capability of silicon nanowire is insensitive to the incident angle [47].

At present, *T-SiNW* is most likely (and expected) to be applied as the block of radial junction devices, e.g., PEDOT:PSS@SiNW [14] or α-Si:H@SiNW solar cells [37]. As we mainly focus on Si/PEDOT:PSS solar cells, here, PEDOT:PSS is chosen as the ambient medium of *T-SiNW*. Fig. 1(b) shows the complex refraction index of silicon and PEDOT:PSS. As the influence of size on the refraction index of silicon material can be ignored [48], the values of bulk silicon are used [49]; the refraction index of PEDOT:PSS is set to be 1.284 [50]. In studying the impact of the ambient medium, the size of *T-SiNW* is chosen to be the same as that used in our previous work, i.e., $D1 = 0.04$ μm, $D2 = 0.12$ μm, and $H = 1.0$ μm [46].

The extinction and absorption performances of *T-SiNW* are calculated via the DDA method by software *ddscat 7.3* [43,44] which performs well and can give accurate results when used to calculate light scattering and absorption properties of silicon [40,42]. In the framework of DDA, the target will be treated as an array of cubes; and each one of the cubes can be regarded as a point dipole. Therefore, the optical properties of the *T-SiNW* can be represented by the response of these point dipoles under an incident electromagnetic wave (light), which can be further solved by an iterative method. In DDA calculations, the inter-dipole spacing (d) and the error tolerance between two adjacent iterative steps (h) are the two factors which determine the calculation accuracy of the DDA method [43,44]. Herein, d and h are set as 3.3 nm and 1.0×10^{-5} respectively, according to our previous tests.

Table 1
Size parameters of *T-SiNW*.

D1(μm)	*D2*(μm)	*H*(μm)	θ/degree	*D1*(μm)	*D2*(μm)	*H*(μm)	θ(degree)
0.04	0.12	1.0	4.58	0.02	0.16	*0.4*	19.85
0.02	*0.10*	1.0	4.58	0.02	0.16	*0.8*	10.00
0.02	*0.14*	1.0	6.87	0.02	0.16	*1.2*	6.68
0.02	*0.18*	1.0	9.15	0.02	0.16	*1.6*	5.01
0.02	*0.22*	1.0	11.42	0.02	0.16	*2.0*	4.01
0.02	*0.26*	1.0	13.69				

The extinction and absorption efficiencies of *T-SiNW* can be defined as $Q_{ext} = C_{ext}/\pi r^2$ and $Q_{abs} = C_{abs}/\pi r^2$, where C_{ext}, C_{abs}, and πr^2 denote the extinction, absorption and real geometric cross-sectional area correspondingly. But it should be mentioned that, as *T-SiNW* has continuous diameters, it requires great care to choose the radius of *T-SiNW*, r, to ensure Q_{ext} and Q_{abs} have specific physical meaning. In this study, we choose the bottom radius of the *T-SiNW* to be r; therefore, Q_{ext} involves a *T-SiNW* occupying an area of πr^2 on the substrate would be capable to collect the light in an area of Q_{ext} multiples of πr^2, and Q_{abs} reflects how much of this collected light can be absorbed in *T-SiNW* itself.

3. Results and discussions

3.1. Impact of the ambient medium on the optical properties of T-SiNW

The optical properties of *T-SiNW* ($D1 = 0.04$ μm, $D2 = 0.12$ μm, and $H = 1.0$ μm) represented by the extinction and absorption efficiency, in air and in PEDOT:PSS are presented in Fig. 2(a). Noticeably, there are five discrete resonances (denoted by filled circles) in the extinction efficiency curves, no matter in air or in PEDOT:PSS. From Fig. 3(a) it can be seen that the number of the resonances increases and the wavelengths of them red-shift concurrently, as the bottom diameter increases; and from Fig. 3(c), it can be observed that the number of resonances and the resonant wavelengths only weakly related to the length of *T-SiNW*. Comprehensively, the resonant wavelengths as well as the number of them are mainly determined by the bottom diameter but have little to do with the length of *T-SiNW*. The discreteness and the size dependencies of the resonances combinedly indicate that the discrete resonances in *T-SiNW* can be attributed to Fano resonance, due to interference between the scattering amplitudes comes from the continuously increased diameters. Another notable feature is that the

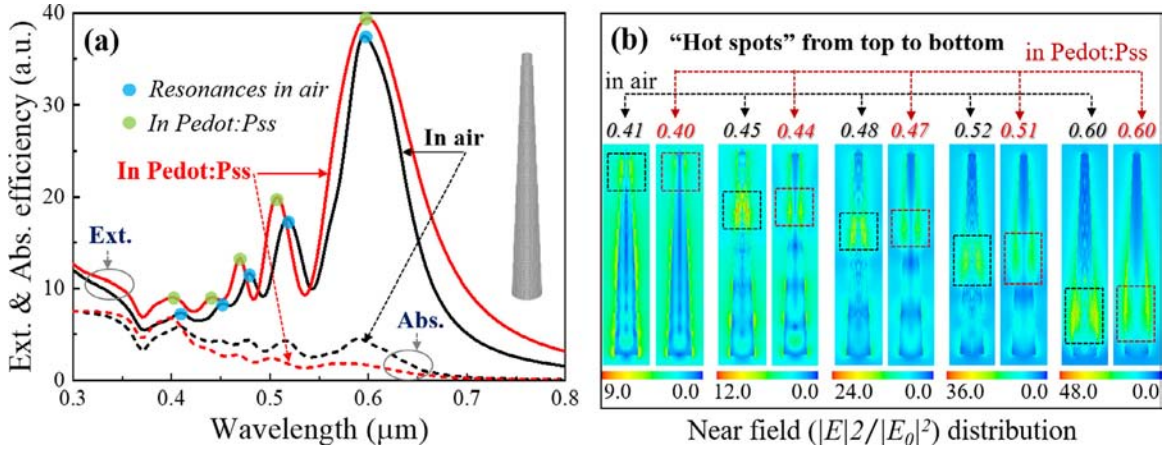

Fig. 2. Comparison of the optical properties of *T-SiNW* in air and PEDOT:PSS. (a) Extinction and absorption efficiency curves in air and PEDOT:PSS, where the blue and green points denote the resonance peaks; (b) Nearfield distribution of the light within and around *T-SiNW* at each resonance wavelength, where the rainbow bars denote the intensity of nearfield light. (For interpretation of the references to colour in this figure legend, the reader is referred to the web version of this article.)

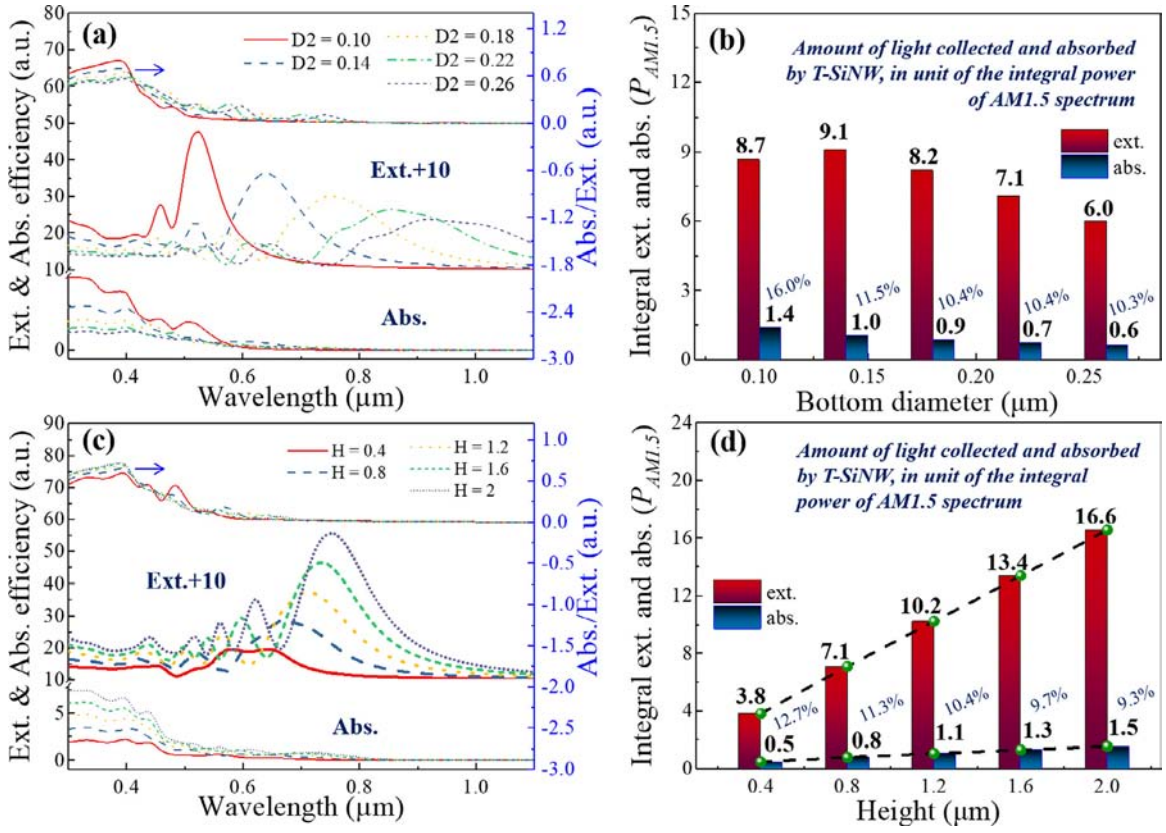

Fig. 3. Extinction and absorption performances of *T-SiNW*. (a) extinction, absorption, and *Abs./Ext.* curves of *T-SiNW* with various *D2*; (b) *AM1.5*-integrated extinction, absorption, and *Abs./Ext.* of *T-SiNW* with various *D2*; (c) extinction, absorption, and *Abs./Ext.* curves of *T-SiNW* with various *H*; (b) *AM1.5*-integrated extinction, absorption, and *Abs./Ext.* of *T-SiNW* with various *H*. The values of the extinction efficiency were added by 10 for a clear illustration.

absorption efficiencies in Fig. 2(a) seem exaggerated smaller than the extinction ones, especially for long-wavelength light. To explain this phenomenon, the nearfield maps ($|E|^2/|E_0|^2$, denote the intensity of nearfield light) which shows the standing waves within/around the frustum at given resonance wavelengths are given in Fig. 2(b). The "hot spots" in the nearfield maps indicate the resonances supported by the different position of the frustum. Such hot spots can be considered as the "collection points" of *T-SiNW*, therefore, the position of the collection points determines the remaining propagation/absorption length.

The most distinct impact of the ambient medium on the optical properties of *T-SiNW* is that the extinction efficiency is enhanced and the peaks blue-shift in PEDOT:PSS, yet the absorption weakens, especially at the waveband of 0.5–0.8 μm where the absorption efficiency is even less than half of that in the air. The blue-shift of the peaks can be attributed to the reduced refraction indices difference between *T-SiNW* and the ambient medium, which will lead to blue-shift of the cut-off wavelength for guide modes supported in *T-SiNW* according to the optical fiber theory. The enhanced extinction efficiency can be ascribed to the slightly extended length of the hot spot for each resonance wavelength, which can couple, thus collect, more amount of light. Such

extended length can be observed by comparing the size of the red and black dashed boxes in the nearfield maps in Fig. 2(b). Meanwhile, the less absorption inside *T-SiNW* in PEDOT:PSS can be attributed to the fact that less light is coupled within but scattered out the *T-SiNW*, as exhibited intuitively in Fig. 2(b) where the intensity of light inside *T-SiNW* in PEDOT:PSS is noticeably weaker than that in air. Nevertheless, further physical reason involving is still not clear.

Based on the above discoveries we can conclude that it is more difficult for *T-SiNW* to perform as a light absorption structure in a radial-junction device in a dielectric medium such as PEDOT:PSS. The light absorption efficiency of *T-SiNW* is sensitive to the refraction indices of the ambient medium; meanwhile, the nearfield light around *T-SiNW* distributes at a wider range with a higher intensity in PEDOT:PSS than that in the air (particularly at the peaks where $\lambda = 0.51$ and 0.6 μm), as shown in Fig. 2(b). Therefore, *T-SiNW* is suitable for the preparation of optical gas sensors and photocatalytic device, whereas the optical signal of molecules adsorbed thereon can be significantly amplified; and further study on the influence law of ambient medium on the optical performance of *T-SiNW* is demanded.

3.2. Impact of size parameters on the optical behaviors of T-SiNW

There are two main application scenarios of *T-SiNW*. The first one is the fabrication of the radial junction device, where *T-SiNW* needs to collect, at the same time, absorb as much light as possible to generate photonic carriers. The second one is the adoption of *T-SiNW* as the light-trapping block, whose only mission is to collect light and transfer it to the substrate. In this scenario, the absorbed light itself should account for as little as possible; meanwhile, the scattered light is better to have large scattering angle. In this section, impacts of size parameters on the optical behaviors of *T-SiNW* including the wavelength-selected light collecting capability, the proportion of light being absorbed itself, as well as the angular distribution of the scattered light, are carefully studied.

3.2.1. The light collecting and absorption performance of T-SiNW

The impact of bottom diameter on the wavelength-selected extinction and absorption curves of *T-SiNW*, as well as the proportion of absorbed light, are shown in Fig. 3(a). Base on the extinction curves, it can be observed that with *D2* increases from 0.1 to 0.26 μm, the wavelengths of the resonance peaks undergo discernible red-shift with diminishing peak intensity. The red-shift of the resonance peak comes from the larger resonance wavelength supported by the increased bottom diameter, and the declining peak intensity can be mainly attributed to the increased denominator (πr^2) in calculating the extinction efficiency where r denotes the bottom radius of *T-SiNW*. From the absorption efficiency curves, it can be observed that the absorption efficiency is always small throughout the whole spectrum; and this value further monotonously decreases as the bottom diameter increases. The ratio between absorption and extinction efficiencies (*Abs./Ext.*) is also illustrated in Fig. 3(a), which should be of better comparability and significance among different *T-SiNWs*. As shown in the figure, the ratio of *Abs./Ext.* is always small when the wavelength is larger than 0.5 μm, disregarding the bottom diameter and extinction peak position. This indicates that *T-SiNW* is indeed unsuitable for the fabrication of radial-junction photovoltaics; and the larger the bottom diameter, the less suitable *T-SiNW* is.

As a prospection to be applied in photovoltaic devices, *T-SiNW* should be scrutinized on its light performance across the whole solar spectrum. The integrals of extinction and absorption curves on *AM 1.5* spectrum (the standard test conditions of a solar cell: 25 °C and irradiance of 1000 W/m^2 with an air mass 1.5 spectrum), as laid out in Fig. 3(b), reveal the light accumulation and light absorption ability of *T-SiNW* to the solar spectrum. Based on the integral of *AM1.5*-weighted extinction efficiency, the light accumulation ability of *T-SiNW* first increases then decreases with its increasing bottom diameter and reaches the maximum when the bottom diameter equals to 140 nm. This phenomenon mostly comes from the widening of the extinction peak and its matching with the photon flux intensity distribution in *AM1.5*: when *D2* = 140 nm, the wavelength with large extinction efficiency corresponds flawlessly to the waveband with strong photon flux intensity in *AM1.5*. Comparing the *AM1.5*-weighted integral of light absorption and the light collecting, one can clearly see the light absorption in *T-SiNW* is very limited; and this absorption value further abates as bottom diameter increases. The reason can be addressed as follows. On the one hand, the matching between extinction peak and the AM1.5 spectrum becomes worse with an increasing bottom diameter; on the other hand, the *Abs./Ext.* ratio gradually decreases, as denoted by the values above the bar of absorption in Fig. 3(b). This decrease in the ratio of *Abs./Ext.* can be attributed to the longer resonance wavelength, which is further due to the increase in bottom diameter; and in accordance with Lambert–Beer Law, light with longer wavelength requires longer propagation distance to be absorbed. Besides, the *Abs./Ext.* ratio reaches a steady state starting from the bottom diameter of 0.18 μm. This is because, as the further increase of bottom diameter beyond this value, the corresponding location of the resonance inside *T-SiNW* is getting close to its lowermost part, whereas the light absorption distance is always short without significant difference.

The impacts of *H* (length) on the wavelength-selected extinction and absorption curves of *T-SiNW*, as well as the *Abs./Ext.* ratio, are shown in Fig. 3(c). The most obvious influence of *H* on the extinction performance of *T-SiNW* is that the extinction peak becomes significantly broadened with the increasing length. This can be explained from the perspective of the leaky mode. The wavelengths at the far left of the peak, which are determined by the cut-off wavelength of the guide mode, are identical. As the length of *T-SiNW* increases, the length of the section corresponding to the same resonance peak on *T-SiNW* also increases; hence, the leaked amount of light increases at a dwindling rate (compared with that in a short section), along with the increasing wavelength. Therefore, the wavelength of the maximum light leakage, corresponding to the extinction peak, red-shifts, and widens the extinction peak. In the second place, the intensity of each resonance peak increases evidently as *H* of *T-SiNW* increases, which can be simply attributed to the fact that the extinction peak intensity is directly proportional to the volume of *SiNW* [7]. Moreover, it can be recognized in Fig. 3(c) that both the light-absorption and the *Abs./Ext.* ratio rise at short waveband, and decrease at long waveband, as the height of *T-SiNW* increases. This is because, at short wavelength, the resonance is primarily supported by the top part of *T-SiNW*, therefore, the collected light obtains a longer propagation distance thus higher *Abs./Ext.* ratio, as the length of *T-SiNW* increases; for the longwave, yet the propagation distance also increases due to the same argument, the red-shift of resonance peak causes an increased distance required for the full absorption of the collected light.

At the same time, the variations of *AM1.5*-integrated extinction and absorption with the changing *H* of *T-SiNW* are also evaluated, as shown in Fig. 3(d). Surprisingly, they are both approximately proportional to *H*, which should be also determined by the fact that the resonance peak intensity is directly proportional to the volume of *T-SiNW*. Meanwhile, as the length of *T-SiNW* increases, we also observe that the ratio *Abs./Ext.* gradually decreases with a further diminishing trend. This result is coherent with the conclusion above based on the same assertion. Theoretically speaking, as the length of T-SiNW further increases, the cone angle decreases as *T-SiNW* gradually evolves into *C-SiNW*. Therefore, the resonance peak intensity would reach a maximum value at the resonance wavelength of *C-SiNW* with a diameter of 0.16 μm; and the ratio *Abs./Ext.* should first decrease and then increase with the increasing length of *T-SiNW*.

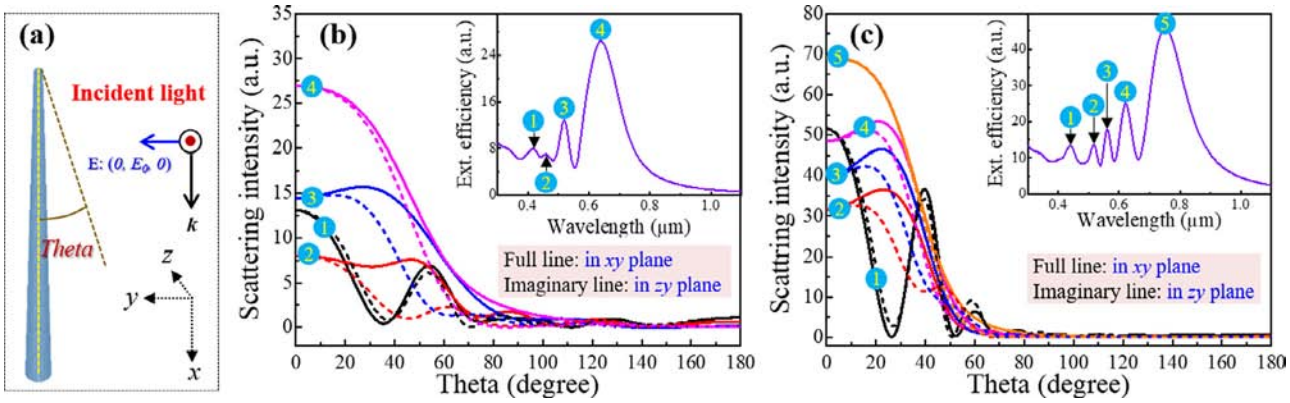

Fig. 4. Angular distribution of the scattered light at representative resonances. (a) illustration of the scattering plane. Results for *T-SiNW* with size (b) *D1* = 20 nm, *D2* = 140 nm, and *H* = 1 μm; 1–4 denote resonances at $\lambda = 0.42$, 0.46, 0.52, and 0.64 μm. (c) *D1* = 20 nm, *D2* = 160 nm, and *H* = 2 μm; 1–5 denote resonances at $\lambda = 0.44$, 0.52, 0.56, 0.62, and 0.76 μm.

3.2.2. The light scattering performance of T-SiNW

As mentioned earlier, the light absorption in *T-SiNW* is weak, especially inside the ambient medium. As a result, *T-SiNW* is unsuitable as the light absorption material in designing photovoltaic and photoelectronic devices. Due to the same reason, the scattering performance of *T-SiNW* becomes more important. Here, the angular distribution curves of scattered light from *T-SiNW* with sizes, *D1* = 20 nm, *D2* = 140 nm, *H* = 1 μm, and *D1* = 20 nm, *D2* = 160 nm, *H* = 2 μm, at representative resonance wavelengths, are given in Fig. 4(b) and (c) respectively.

Fig. 4(b) illustrates the angular distribution of scattered light at different resonance wavelengths from *T-SiNW* with *D1* = 20 nm, *D2* = 140 nm, and *H* = 1 μm. First of all, all scattered light is within the range of $\theta < 90°$, i.e., falls in the category of forwarding scattering. In detail, the angular distribution range of scattered light by *T-SiNW* is largely expanded from $\theta < 30°$ to $\theta < 60°$ compared with that for *C-SiNW* [42]; at the same time, it also exhibits the noticeable amount of scattered light at a range of $\theta = 60°$–$90°$, especially for light with a long wavelength. This feature is extremely beneficial as it means *T-SiNW* can convert the light from longitudinal transmission to lateral transmission. Combining the above-mentioned features, *T-SiNW* has extraordinary light collecting ability across the whole spectrum; and most of the collected light is forward-scattered except a slight amount of it being absorbed; it can convert the light from longitudinal transmission to lateral transmission. Therefore, *T-SiNW* bears exceptional light-trapping structure for photovoltaic and photoelectronic devices.

Angular distribution of scattered light also correlates the resonance wavelength if we look into more details. Shorter wavelength has a more confined scattered light angular distribution; whereas the longer wavelengths have a more expanded scattered light angular distribution. As it can be speculated, light with long wavelength would principally be scattered at the bottom of *T-SiNW*, being converted into the lateral transmission. This demands special consideration when designing new photovoltaic devices. Moreover, scattering intensity and angular distribution in different scattering planes are also different. For the light of the shortest wavelength, the light intensities in two scattering planes are almost identical as shown in Fig. 4(b). This can be ascribed to the fact that the short-wave resonance takes place at the very thin part of *T-SiNW,* which provides big spacial restrictions for dipole oscillation excited by the incident light. With such restrictions, the polarized incident light can be alternated into an essentially natural one. As the wavelength increases, the part on *T-SiNW* with a larger diameter range provide a weakened spacial restriction; meanwhile, the part is still too thin and can only support a single mode. Therefore, the difference in scattering intensity is conspicuous in two perpendicular scattering planes. When the resonances are supported by the bottom part of *T-SiNW*, the diameter of this part is large enough to support two or more kinds of modes, as illustrated by the peaks with $\lambda = 0.6$ μm and 0.64 μm in the first row of Fig. 2(b); consequently, the difference of scattering intensity in two scattering planes, in turn, becomes less discernible.

Fig. 4(c) delineates the angular distribution of light scattered by *T-SiNW*, with *D1* = 20 nm, *D2* = 160 nm, *H* = 2 μm, at different resonance wavelengths. Correlating the preceding case of *T-SiNW* with *H* = 1 μm, length can be found out to have a prevalent impact on the angular distribution of scattered light. The most noticeable effect is that the scattered angular distribution narrows down with the increase of *H*, which is quite understandable as *T-SiNW* resembles *C-SiNW* better as *H* increases. Accordingly, we can conclude that, when being used for light-trapping, *T-SiNW* is preferably to be short and thick (i.e. with large cone angle). Such *T-SiNW* would, at the same time, absorb less light, and expand the scattered light angular distribution to the greatest degree. Furthermore, from Fig. 4(c) it can be observed that *T-SiNW* with increased length demonstrates excellent effectiveness on changing the polarized incident light into a natural one, especially for long wave light: there is almost no difference between the intensities of light in two scattering planes for resonance at $\lambda = 0.76$ μm.

4. Conclusion

In summary, the effect of the ambient medium, PEDOT:PSS, and structure parameters, bottom diameter and length, on the optical performances of *T-SiNW* are carefully studied based on numerical simulations using the DDA method. First of all, in PEDOT:PSS, the absorbed light in *T-SiNW* is much less than that in air, especially in waveband with $\lambda > 0.5$ μm where the amount of absorbed light is even less than half of that in air. This can be attributed to the less amount of light being coupled within *T-SiNW*. Then, the scattered light by *T-SiNW* mainly distributes in an angle range of 0–60° (quite wider than that in air, i.e. 0–30°), which is very useful as it means *T-SiNW* in PEDOT:PSS can convert the light from longitudinal transmission to lateral transmission. These two features indicate that *T-SiNW* is a desirable light-trapping structure especially in the ambient medium, which can be used in *T-SiNW*-based solar cells. Besides, the nearfield light around *T-SiNW* looks stronger in a wider area than that in air, especially at the wavelengths of 0.51 μm and 0.6 μm. This is helpful for the fabrication of gas sensors as the optical response of gas molecules adsorbed on the surface of *T-SiNW* can be further amplified.

Size parameters show obvious impacts on the optical behaviors of *T-SiNW*. With the increased bottom diameter of *T-SiNW*, its extinction peaks red-shift as the resonance is supported by its increased diameter on the bottom part. Then, in waveband with $\lambda > 0.5$ μm, the ratio *Abs./Ext.* in *T-SiNW* is always small and almost independent of the bottom diameter. In addition, the angular distribution of the scattered light by *T-SiNW* can be broadened as the bottom diameter (taper

angle) increases. Consequentially, *T-SiNW* with larger bottom diameter is more desirable for light-trapping. From the *AM1.5*-weighted integrals of extinction efficiency, it can be concluded that the optimized bottom diameter of *T-SiNW* is 140 nm. It is found that the light-collecting and -absorption multiples of *T-SiNW* are both proportional to its length thus volume; meanwhile, the scattering angle distribution narrows with increasing *T-SiNW* length. As a result, short *T-SiNW* with large bottom diameter is best for light-trapping. As *T-SiNW* has more resonance peaks and is more sensitive in optical behaviors than *C-SiNW*, it is very promising to be utilized in fabricating pure optically-sensitive gas sensors. Further study on the influence of varied ambient media on the optical behaviors of *T-SiNW* and to further exploit its potential applications should be a very interesting research direction.

Acknowledgments

This work was supported partially by the National Natural Science Foundation of China (Grant Nos. 51402106, 91333122, 11504107, and 51372082); the Fundamental Research Funds for the Central Universities, China (2016JQ01, 2015ZZD03, and 2015ZD07).

References

[1] Y. Ding, R. Magnusson, Resonant leaky-mode spectral-band engineering and device applications, Opt. Express 12 (2004) 5661–5674.
[2] R. Paniagua-Dominguez, G. Grzela, J.G. Rivas, J.A. Sánchez-Gil, Enhanced and directional emission of semiconductor nanowires tailored through leaky/guided modes, Nanoscale 5 (2013) 10582–10590.
[3] Y. Yu, L. Cao, Coupled leaky mode theory for light absorption in 2D, 1D, and 0D semiconductor nanostructures, Opt. Express 20 (2012) 13847–13856.
[4] A.E. Miroshnichenko, S. Flach, Y.S. Kivshar, Fano resonances in nanoscale structures, Rev. Modern Phys. 82 (2010) 2257.
[5] B. Luk'yanchuk, N.I. Zheludev, S.A. Maier, N.J. Halas, P. Nordlander, H. Giessen, C.T. Chong, The Fano resonance in plasmonic nanostructures and metamaterials, Nat. Mater. 9 (2010) 707.
[6] Y.F. Li, M.C. Li, R.K. Li, P.F. Fu, T. Wang, Y.N. Luo, J.M. Mbengue, M. Trevor, Exact comprehensive equations for the photon management properties of silicon nanowire, Sci. Rep. 6 (2016) 24847.
[7] Y. Li, L. Yue, Y. Luo, W. Liu, M. Li, Light harvesting of silicon nanostructure for solar cells application, Opt. Express 24 (2016) A1075–A1082.
[8] S.-K. Kim, R.W. Day, J.F. Cahoon, T.J. Kempa, K.-D. Song, H.-G. Park, C.M. Lieber, Tuning light absorption in core/shell silicon nanowire photovoltaic devices through morphological design, Nano Lett. 12 (2012) 4971–4976.
[9] K.T. Fountaine, C.G. Kendall, H.A. Atwater, Near-unity broadband absorption designs for semiconducting nanowire arrays via localized radial mode excitation, Opt. Express 22 (2014) A930–A940.
[10] J. Zhu, Z. Yu, G.F. Burkhard, C.-M. Hsu, S.T. Connor, Y. Xu, Q. Wang, M. McGehee, S. Fan, Y. Cui, Optical absorption enhancement in amorphous silicon nanowire and nanocone arrays, Nano Lett. 9 (2008) 279–282.
[11] B. Hua, B. Wang, M. Yu, P.W. Leu, Z. Fan, Rational geometrical design of multi-diameter nanopillars for efficient light harvesting, Nano Energy 2 (2013) 951–957.
[12] H. Jeong, H. Song, Y. Pak, I.K. Kwon, K. Jo, H. Lee, G.Y. Jung, Enhanced light absorption of silicon nanotube arrays for organic/inorganic hybrid solar cells, Adv. Mater. 26 (2014) 3445–3450.
[13] S.S. Yoon, D.Y. Khang, High efficiency (> 17%) si-organic hybrid solar cells by simultaneous structural, electrical, and interfacial engineering via low-temperature processes, Advanced Energy Materials 8 (2018) 1702655.
[14] J. He, P. Gao, M. Liao, X. Yang, Z. Ying, S. Zhou, J. Ye, Y. Cui, Realization of 13.6% efficiency on 20μm thick si/organic hybrid heterojunction solar cells via advanced nanotexturing and surface recombination suppression, ACS Nano 9 (2015) 6522–6531.
[15] R.H. Coridan, K.A. Arpin, B.S. Brunschwig, P.V. Braun, N.S. Lewis, Photoelectrochemical behavior of hierarchically structured Si/WO3 core–shell tandem photoanodes, Nano Lett. 14 (2014) 2310–2317.
[16] S. Xu, Y. Qin, C. Xu, Y. Wei, R. Yang, Z.L. Wang, Self-powered nanowire devices, Nature Nanotechnol. 5 (2010) 366.
[17] S. Sett, S. Sengupta, N. Ganesh, K. Narayan, A. Raychaudhuri, Self-powered single semiconductor nanowire photodetector, Nanotechnology 29 (2018) 445202.
[18] B. Tian, X. Zheng, T.J. Kempa, Y. Fang, N. Yu, G. Yu, J. Huang, C.M. Lieber, Coaxial silicon nanowires as solar cells and nanoelectronic power sources, nature 449 (2007) 885.
[19] I.E. Zadeh, A.W. Elshaari, K.D. Jöns, A. Fognini, D. Dalacu, P.J. Poole, M.E. Reimer, V. Zwiller, Deterministic integration of single photon sources in silicon based photonic circuits, Nano Lett. 16 (2016) 2289–2294.
[20] B. Chen, H. Wu, C. Xin, D. Dai, L. Tong, Flexible integration of free-standing nanowires into silicon photonics, Nat. Commun. 8 (2017) 20.
[21] S. Goodnick, R. Nemnich, A. Korkin, Focus on electronics photonics and renewable energy, Nanotechnology 29 (2018) 360201.
[22] G. Ducournau, Silicon photonics targets terahertz region, Nat. Photonics 12 (2018) 574.
[23] R.R. Singh, N. Malviya, V. Priye, Parametric analysis of silicon nanowire optical rectangular waveguide sensor, IEEE Photonics Technol. Lett. 28 (2016) 2889–2892.
[24] R.R. Singh, V. Priye, Silicon nanowire optical rectangular waveguide biosensor for DNA hybridization, IEEE Photonics Technol. Lett. 30 (2018) 1123–1126.
[25] R.R. Singh, A. Singh, A. Gautam, V. Priye, Vertical silicon nanowire-based optical waveguide for DNA hybridization biosensor, in: Quantum Sensing and Nano Electronics and Photonics XVI, International Society for Optics and Photonics, 2019, p. 109262M.
[26] I. Zardo, S. Conesa-Boj, S. Estradé, L. Yu, F. Peiro, P.R. i Cabarrocas, J. Morante, J. Arbiol, A.F. i Morral, Growth study of indium-catalyzed silicon nanowires by plasma enhanced chemical vapor deposition, Appl. Phys. A 100 (2010) 287–296.
[27] J.R. Maiolo, B.M. Kayes, M.A. Filler, M.C. Putnam, M.D. Kelzenberg, H.A. Atwater, N.S. Lewis, High aspect ratio silicon wire array photoelectrochemical cells, J. Am. Chem. Soc. 129 (2007) 12346–12347.
[28] Ruike Li, M. Li, Y. Li, P. Fu, Y. Luo, H. Rui, D. Song, J.M. Mbenque, Co-catalytic mechanism of Au and Ag in silicon etching to fabricate novel nanostructures, RSC Adv. 5 (2015) 96483–96487.
[29] F. Bai, M. Li, D. Song, H. Yu, B. Jiang, Y. Li, Metal-assisted homogeneous etching of single crystal silicon: A novel approach to obtain an ultra-thin silicon wafer, Appl. Surf. Sci. 273 (2013) 107–110.
[30] F. Bai, M. Li, R. Huang, Y. Yu, T. Gu, Z. Chen, H. Fan, B. Jiang, Wafer-scale fabrication of uniform Si nanowire arrays using the Si wafer with UV/Ozone pretreatment, J. Nanoparticle Res. 15 (2013) 1–7.
[31] K.-Q. Peng, X. Wang, L. Li, Y. Hu, S.-T. Lee, Silicon nanowires for advanced energy conversion and storage, Nano Today 8 (2013) 75–97.
[32] Y. Wang, T. Wang, P. Da, M. Xu, H. Wu, G. Zheng, Silicon nanowires for biosensing, energy storage, and conversion, Adv. Mater. 25 (2013) 5177–5195.
[33] T. Song, S.-T. Lee, B. Sun, Silicon nanowires for photovoltaic applications: The progress and challenge, Nano Energy 1 (2012) 654–673.
[34] K.Q. Peng, S.T. Lee, Silicon nanowires for photovoltaic solar energy conversion, Adv. Mater. 23 (2011) 198–215.
[35] P. Krogstrup, H.I. Jørgensen, M. Heiss, O. Demichel, J.V. Holm, M. Aagesen, J. Nygard, A.F. i Morral, Single-nanowire solar cells beyond the Shockley–Queisser limit, Nat. Photonics 7 (2013) 306.
[36] C. Zhang, Z. Yang, K. Wu, X. Li, Design of asymmetric nanovoid resonator for silicon-based single-nanowire solar absorbers, Nano Energy 27 (2016) 611–618.
[37] L. Yu, S. Misra, J. Wang, S. Qian, M. Foldyna, J. Xu, Y. Shi, E. Johnson, P.R. i Cabarrocas, Understanding light harvesting in radial junction amorphous silicon thin film solar cells, Sci. Rep. 4 (2014) 4357.
[38] Y. Zhan, J. Zhao, C. Zhou, M. Alemayehu, Y. Li, Y. Li, Enhanced photon absorption of single nanowire α-Si solar cells modulated by silver core, Opt. Express 20 (2012) 11506–11516.
[39] L. Cao, J.S. White, J.-S. Park, J.A. Schuller, B.M. Clemens, M.L. Brongersma, Engineering light absorption in semiconductor nanowire devices, Nat. Mater. 8 (2009) 643.
[40] Y. Li, W. Liu, Y. Luo, M. Cui, M. Li, Oxidation of silicon nanowire can transport much more light into silicon substrate, Opt. Express 26 (2018) A19–A29.
[41] X. Li, N.P. Hylton, V. Giannini, K.-H. Lee, N.J. Ekins-Daukes, S.A. Maier, Bridging electromagnetic and carrier transport calculations for three-dimensional modelling of plasmonic solar cells, Opt. Express 19 (2011) A888–A896.
[42] Y. Li, M. Li, D. Song, H. Liu, B. Jiang, F. Bai, L. Chu, Broadband light-concentration with near-surface distribution by silver capped silicon nanowire for high-performance solar cells, Nano Energy 11 (2015) 756–764.
[43] B.T. Draine, P.J. Flatau, Discrete-dipole approximation for scattering calculations, J. Opt. Soc. Amer. A 11 (1994) 1491–1499.
[44] P. Flatau, B. Draine, Fast near field calculations in the discrete dipole approximation for regular rectilinear grids, Opt. Express 20 (2012) 1247–1252.
[45] C. Ungureanu, R.G. Rayavarapu, S. Manohar, T.G. van Leeuwen, Discrete dipole approximation simulations of gold nanorod optical properties: Choice of input parameters and comparison with experiment, J. Appl. Phys. 105 (2009) 102032.
[46] Y. Li, M. Li, P. Fu, R. Li, D. Song, C. Shen, Y. Zhao, A comparison of light-harvesting performance of silicon nanocones and nanowires for radial-junction solar cells, Sci. Rep. 5 (2015) 11532.
[47] L. Cao, P. Fan, A.P. Vasudev, J.S. White, Z. Yu, W. Cai, J.A. Schuller, S. Fan, M.L. Brongersma, Semiconductor nanowire optical antenna solar absorbers, Nano Lett. 10 (2010) 439–445.
[48] K.W. Kolasinski, Silicon nanostructures from electroless electrochemical etching, Curr. Opin. Solid State Mater. Sci. 9 (2005) 73–83.
[49] E.D. Palik, Handbook of Optical Constants of Solids, Academic press, 1998.
[50] G. Pathak, Z. Krasińska-Krawet, L. Szyk-Warszyńska, D. Čakara, Doping of poly (3, 4-ethylenedioxythiophene): poly (styrenesulfonate) films studied by means of electrochemical angle spectroscopic ellipsometry, Thin Solid Films 651 (2018) 31–38.